

Characterization of a mild steel by its mutual Tensile Mechanical and Micromagnetic emission response after corrosion in NaCl – water Solution: a combined semiquantitative approach

A. F. Altzoumailis^{a*}, V. N. Kytopoulos^b

^{a*} School of Chemical Engineering, National Technical University of Athens, 5 Heroes of Polytechnion Avenue 157 73 Athens, GREECE.

^bSchool of Applied Mathematical and Physical Sciences, National Technical University of Athens, 5 Heroes of Polytechnion Avenue 157 73 Athens, GREECE.

Received: June 14, 2021 Revised: July 19, 2021. Accepted: July 26, 2021. Published: July 28, 2021.

Abstract: - In this work, the influence of corrosion – induced hydrogen accumulation on a stressed low- carbon steel after exposure to NaCl - water solution was investigated by means of its combined tensile mechanical and Micromagnetic emission (ME) - response. The investigation was conducted by employing certain relevant parameters and processes of mechanical and magnetic microstructural changes. The mechanical and Micromagnetic response data were reduced to the ultimate tensile strength as well as to maximum (ME) - response respectively where certain critical- characteristic microstructural- transitional changes take place. Under these conditions and by an appropriate procedure of “consecutive - selective discrimination steps” of the related affecting factors their differential influence on the mechanical and ME – response was better revealed, compared and analyzed. In this manner it was demonstrated that the detrimental influence of cumulative hydrogen arises

in from of mechanical embrittlement which can be related to a parallel magnetic hardening trend of the material. The explanations are given on the basis of highly localized and competitive or opposing processes of void initiation- growth and stress relieve, resulting by a common lattice diffusion, as well as moving dislocation- aided transport of hydrogen to the affected sites. Within the frame of the above findings it was shown that the ME- response presents, compared with mechanical response, an increased sensitivity making the first a superior technique in early detecting hydrogen- assisted microstructural damage in loaded steel components.

Key-words: - Hydrogen accumulation, j-parameter, ME- response, mechanical response, specific sensitivity.

I INTRODUCTION

In industrial situations one often meets the combination of both a damaging environment and applied load which may lead to premature fracture of parts of

structural steel components. For this reason, today, there is a growing need for non-destructive inspection and characterization of such components under sustained loading conditions where early detection of environmental-induced microstructural damaging defects plays a distinct role. In practice, in-service creep-like loading conditions may adequately be simulated by quasi-static, progressive loading test, conducted under a suitable strain rate as low as $\leq 10^{-4}$ /s. of used low-carbon steel (%)

Thus, of great importance are for example such tests concerning hydrogen-assisted creep rupture in certain steels where the rupture life, t_R , at given temperature and stress is evaluated for short-life situations such as rocket engine nozzle with $t_R \approx 100$ sec or turbine blade in military aircraft engine with $t_R = 100$ hrs. Further related tests in the field of long-life material applications such as in nuclear power plant, where critical parameter of minimum creep rate may be influenced by dominating hydrogen-assisted creep-like pervasive damaging mechanisms, are of increasing importance. In the same field of application high strength steel component of marine plants are known to be very susceptible to hydrogen embrittlement and cracking due to aggressive-corrosive sea water environment. Therefore, under the above condition different type of failure may exist such as stress-corrosion cracking, delay hydrogen cracking, static fatigue-fracture, creep rupture, weld-cold cracking, season cracking etc. It becomes evident that an early and correct detection and interpretation of defects produced under these conditions of failure is of significant importance. Because of its uniqueness in utilizing certain characteristic-inherent phenomena of ferromagnetic steels, micromagnetic emission response (ME), known as magnetic Barkhausen Noise, is appropriate and reliable technique to detect such defects whose creation may be simulated by a wide spectrum of progressive quasi-

static loading, beginning from initial elastic-plastic, to gross-or progressive yielding and necking down state and terminated close to final fracture instant of material. Additionally, this technique, unlike ultrasonic, X-ray and other physical ones [1] do not require expensive, ultra-high resolution electronics and optics and other experimental attachments and as such is a quick and cheap technique. At the same time, by combinations of variant 'sub techniques' [2], this seems to be one of the most versatile and reliable method for characterization of steels. Today, despite very extensive research in this field, hydrogen embrittlement and other hydrogen-assisted damage phenomena, due to their complexity, are not yet well understood and need further investigations. In view of the above-mentioned complexities of the problems we try to introduce some new relevant approaches to these problems on the basis of an applied stress-triggered state in form of a combined mechanical and ME-response of the cumulative hydrogen-affected steel. More concretely, the subject of present study is to introduce and apply a such approach, where among others, by means of a appropriate reduction procedure consisting in a "selective discrimination" of the influential factors their differential-competitive contribution to damage can better be revealed compared and analyzed. By this approach it is hoped to gain further valuable information about pervasive hydrogen-assisted damage processes occurring in loaded steels. Because of steps the first time of application of the present approach it is suggested to use as reference testing material a simple modelling steel where most of its intrinsic microstructural-metallurgical defects had been annealed out or eliminated and the prepared specimens were well-characterized from the beginning. With respect to this a prime candidate for such a material appears to be Armco-type low-carbon steels which was selected to be used for the scope of present study.

<i>C</i>	<i>Mn</i>	<i>Si</i>	<i>Ni</i>	<i>Cr</i>	<i>Mo</i>	<i>S</i>	<i>P</i>	<i>N</i>
<i>0.04</i>	<i>0.44</i>	<i>0.015</i>	<i>0.016</i>	<i>0.015</i>	<i>0.002</i>	<i>0.016</i>	<i>0.02</i>	<i>0.004</i>

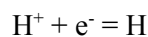
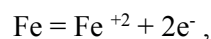
Table1. The chemical composition

II EXPERIMENTAL PROCEDURE

A block diagram of the experimental set up used for the measurement of micromagnetic emission or Barkhausen noise response is shown in Figure [1]. The magnetic excitation field was directed parallel to principal axial stress and parallel to specimen axis. The estimated depth of minimum penetration of magnetizing field was roughly 1mm, whereas the depth of ME origin about 50µm. In figure 1a the frequency response of the Barkhausen noise sensor is illustrated. This response can be subtracted by the Barkhausen sensor in order to get the associated signal coming from the subsurface layer of the specimen under test. A current from a sweep controller circuit was fed to a bipolar high current generator to produce a symmetric bipolar triangular wave form. The applied sampling frequency was 100 KHz and maximum magnetic induction field of the excitation was about 20G. The ME signal at 10 Hz magnetic excitation was acquired by a 2 mm ferrite surface probe which had 1000 turns and then amplified to 40dB using a low noise amplifier . The amplified signal was band –pass filtered in the range 500Hz to 10 KHz for eventual voltage and spectral analysis measurements. The total number of

Barkhausen counts (events), and the corresponding rms-voltage level was measured for one second of magnetization frequency using the counter processing module of the given apparatus. Barkhausen signal is selected through a 500-Hz high-pass filter, which ensures the rejection of low – frequency components of signal linked with B= f (H) hysteresis loop. An adequate threshold voltage was used to eliminate low- amplitude circuit noise and other background noise. The chemical composition of the used material is given in table [1]. The material was a polycrystalline one with average grain size of about 35 µm. This material was received in form of sheets produced by cold rolling and subsequent adequate annealing for internal stress- relief. The surfaces of the specimens were finished first by grinding with 600 grid paper. Any as received surface and subsurface residual stresses as well as and caused by grinding were eliminated by convenient chemical etching and/ or electropolishing procedure thus removing about 100 µm of surface material. Measurements have shown that virtually vanishing residual stresses of the order of 5MPa were still present. The related measurements were performed with equipment using CrKa radiation and the standard dVs.sin²ψ technique [3]. The specimen had dogbone-type geometry where thickness was 2 mm, width 10 mm and the effective gauge

length 100 mm. The samples were subjected to uniaxial tensile test at room – temperature nominal low strain rate, $10^{-4}/s$, using a universal testing machine of Instron- type. The ultimate stress was 380MPa and the off-set yield stress (0.2%) was 190 MPa. The specimen was continuously loaded and data were taken at convenient time intervals under load. Before testing, the samples were exposed to a corrosive environment produced by a continuously sprayed 3.5% NaCl aqueous solution in a Salt Spray Fog (SSF) apparatus. All corrosion experiments were performed at room temperature for 100, 200, 600, 1000 hours. The final corrosion product was a brownish, scale – like layer formed on the specimen surface. This layer was a loosely adhering one containing in a great part, as obtained by X-ray diffraction analysis, a ferric oxyhydroxide $FeO(OH)$ component. This product in turn was removed by dry air blast and soft natural bristle brush revealing underneath a black and strong adhering layer in form of magnetite (Fe_3O_4) product. During the magnetite formation the production of atomic hydrogen takes place by the following basic reactions [4].



Afterwards, the magnetite layer was removed by appropriate chemical etching procedure. Otherwise this ferromagnetic layer would appreciably obscure the derived magnetic signal emitted by the near- surface layers of specimens. Subsequent X- ray diffraction analysis of specimen surfaces resulted in no significant changes in the initial residual stress state. Thereafter, the specimens were subjected to testing produce as explained before

III RESULTS AND DISCUSSION

In Figure (2), the tensile engineering stress- strain curves for non-corroded and corroded specimens with respect to time of exposure in NaCl- water solution are presented. Thus, one can clearly see the overall shift of curves to lower fracture strain with increasing exposure time. This fact may be indicative of occurrence of an embrittlement of the material. With respect to this fact, one should mention that similar behavior of steels, due to hydrogen cathodic charging, was obtained elsewhere [5]. Moreover, in recent studies such a behavior of a low carbon steel was attributed to hydrogen – assisted embrittlement [6, 7]. This was possible by employing detailed microfractographic analysis by Scanning Electron Microscopy [SEM] [6-11]. Thus, the observed present behavior of the curves in Figure (2) can be attributed to hydrogen – assisted embrittling processes. At this place one should remember that hydrogen embrittlement can in general be accepted as a mechanical environmental failure occurring in the presence of atomic/ molecular hydrogen in metals and alloys in dissolved or absorbed form along with internal residual or static stresses. Thus, hydrogen may be produced among others by an electrochemical corrosion reaction at the surface and can afterwards enter into the steel in atomic/molecular form. Details about this reaction were given in the experimental section. Once entered into the steel hydrogen is accumulated, in a first instance, at the affected stress gradients sites and internal interfaces through a rapid lattice diffusional transport due to its very small size and hence its large fugacity. Nevertheless, of potentially greater significance is the fact that, as shown calculations, hydrogen transport rates in association with dislocation motion can be several orders of magnitude greater than that associated with lattice diffusion [8]. Hence, a moving dislocation – aided hydrogen transport may be

stimulated during slow strain rate test of plastic deformation thus giving a respectable contribution to hydrogen embrittlement [9, 10]. By its complexity, however, hydrogen embrittlement is not yet fully understood, although several theoretical modelling approaches have been proposed in this directions [8, 10-12]. With respect to this, it should be mentioned that the basis of all models is the existence of a highly localized, combined mechanisms of hydrogen – assisted void initiation and growth as well as stress- relief resulting in lowering the interatomic cohesive strength and specific surface energy [12].

Furthermore, the behavior of engineering stress-strain curves shown in Figure (2), can further be characterized by regions I and II separated by the strain point at which ultimate tensile stress (strength) occurs, denoted in the Figure by e_u . This is a critical strain reflecting the onset of a plastic instability phenomenon in form of a localized necking of specimen gauge. This may happen because during progressive plastic deformation the material hardens, thereby making it more resistant to further deformation. However, a critical point is reached, where the limiting strain – hardening capacity of the material is exhausted and local area contraction at the weakest point along the gauge length is no longer balanced by an associated increase in the materials strength. Afterwards, at this point, due to presence of high triaxle stress fields, a critical volume damage in form of microcracks and cavities are produced which can coalesce with one another leading to a necking down and final fracture of material. Furthermore, from the theory of strength of materials it is known that at the ultimate engineering tensile strength point the characteristic relation $\epsilon_c = \ln(e_u + 1) = n$ exist, where e_u is the associated ultimate engineering strain and ϵ_c the calculated critical true strain [8, 13]. The so calculated basic parameter, n , is the plastic strain hardening rate exponent in the Hollomon formula, $\sigma = H\epsilon^n$ best –fitted to the experimental true stress-strain curve where H is the corresponding amplitude constant. [13]. Consequently, one should point out that

due to this parameter (n) of the two above presented relations the previously mentioned strain hardening and elastic - plastic volume damage process may suitably be “coupled”, thus giving to this parameter a combined physical meaning of the evolution of internal state of microstructural changes. Therefore, we introduce the parameter $n_o/n_i = \tilde{n}$, as a reduced mechanical response number, where n_o denotes the absolute mechanical response number of the non- corroded (hydrogen – free material) and n_i the same number of corroded material for hydrogen accumulation for exposure time $t_i > 0$. As such, this reduced parameter may simulate a process of time scaling in the sense that, by its increase, the critical (mechanical) damage accumulation may be “detected” in early stages of plastic deformation. In other words, this could mean a kind of increased ability or sensitivity of mechanical response to characterize mechanical degradation of material.

Now, following the scope of the present work, one can try to obtain additional, valuable information about hydrogen effects in stressed steel by investigating its combined micromagnetic emission and mechanical tensile stress-strain response. This is performed by employing certain characteristic activity processes occurring in ferromagnetic materials determined by jumping displacement of magnetic domain walls causing the micromagnetic emission effect or Barkhausen noise. This is measured by particular quantitative and qualitative parameters such as the emission rate of events and root –mean – square voltage (V_{rms} – energy) signal respectively. Micromagnetic emission is produced by the irreversible movement of domain walls during an applied magnetization excitation cycle. Moving domain walls are pinned temporarily by microstructural inhomogeneities or defects and then released by the increasing applied magnetic field. The resulting discrete-abrupt changes in the magnetization are detected in form of voltage pulses (counts) induced in an external pick-up (search) coil. Inhomogeneities such as dislocation, precipitation, microcracks as well as void and / or cavities may act as effective barriers to domain wall motion. Moreover,

due to the magnetostrictive interaction, applied and / or residual stresses may also markedly influence the intensity of ME – emission response. More details about the ME or Barkhausen noise phenomenon and measurement procedure are given elsewhere [2]. In particular, such measurements are shown in Figure (3) where both kinds of signal parameters are plotted together versus applied strain. In this manner certain apparent “inconsistency” between these parameters may be observed in the sense that for certain given strain points or regions an opposite trend in their behavior results in the sense that an increase in the count signal is associated by a decrease in the V_{rms} signal. Similar trends were also observed in [7], where no further explanation are given. This apparent “problem” could lead to a more or less ambiguous interpretation of the data. To overcome, at least in part, this “problem” we try to adopt a more relevant ME-response parameter denoted as $j = V_{rms} / N$, where V_{rms} is the measured root-mean-square voltage signal and N the corresponding number of measured counts (pulses). Initially it is seen that this parameter is a function of both kind of signals and as such gives a measure of a rough average of weak and strong event. These events could be separated by respective puls – height – spectrum analysis, procedure being beyond the scopus of present investigation [2]. In particular, however, the square of V_{rms} amplitude is correlated to the event (pulse) energy rate and provides a more weightage to strong energetic events. Nevertheless it is suggested to accept the above introduced j - parameter as a nominal absolute measure of the strength of domain wall jump of micromagnetic activity. In regard to micromagnetic jump activity it should be noted that the strength (intensity) of the domain wall jump between pinning sites is determined by a combined effect of jump length, jump velocity and domain structure producing thus a particular, local magnetic volume change [2]. It follows that this volume change becomes an “input” for the induced and detected electric pulse integrated over its duration time.

Thereafter, preparative measurements have shown that the proposed parameter (j) seems to be robust in the sense that, under same conditions, it is little affected by changing the measurement points on the specimen surface and specialty including lift-off effects simulated by variation of inclination angles between probe and surface normal. In this aspect statistical evaluations conducted by means of standard deviation have shown a much better behavior of the j -parameter compared to the count and / or V_{rms} signal data taken separately. Thus, in the following we try to present and discuss the obtained data by means of the absolute as well as by relative or reduced form of measured ME- response. Hence, the parameter $\bar{j} = j_i / j_0$, is the reduced or relative form of ME – response where j_0 and j_i represents the corrosion – free and corrosion – related absolute ME-response in function of hydrogen accumulation time $t = 0$ and $t_i > 0$ respectively. This is shown in Figure (4) where this response of the not stressed steel in function of hydrogen accumulation time is plotted. Thus, one can observe the formation of a minimum point of this response for time of about $t = 200$ hrs. A reasonable hypothetical explanation of this behavior could be given by introducing the regions I* and II* as shown in this Figure. As such region I* is characterized by a hydrogen – assisted void growth controlling process, whereas region II* by a hydrogen – assisted stress – relief controlling process. Consequently, at this minimum point a subtle counterbalance between these two processes should exist. Therefore, the resulted magnetic responses on these opposing processes can most probably be explained as follows: the growth of microvoids which reflect the creation of new open internal surfaces or interfaces having increased specific surface energy [14], may act as additional energy barriers in form of pinning sites for magnetic domains walls. This would result in an associated net decrease in the reduced – ME – response of micromagnetic activity. At the same time, stress relief tends to reduce the magnetostriction-included magnetoelastic interaction of domain walls with pinning sites in stimulating a net

increase in the nominal (absolute) ME-response.

In the representative series of figures (6,7,8,9) the obtained absolute ME-response parameter, j , versus applied strain for corrosion – free and certain representative states of given hydrogen accumulation time is presented. For the sake of following constructive discussions the related engineering stress- strain curve for each j curve was inserted. As shown each stress-strain curve is characterized by the earlier introduced ranges I and II separated by the ultimate critical strain ε_{cr} . Thereafter, one can so observe the interesting behavior of an almost monotonic increase in the ME – response up to the magnetic critical strain point, ε_{cr} after which an almost monotonic decrease, up to the final fracture follows. Thereafter, we focus now our attention, at first, on the formed maximum value, $j^{(max)}$ in this response which could better be explained, as shown for example in fig (6), by introducing regions I* and II*, separated by the magnetic critical strain point ε_{*c} . Keeping in mind that applied tensile stresses are opposing to plastic strain damaging effects with respect to ME-response [16-21] the formation of region I* might predominantly be attributed to an applied stress control whereas the formation of region II* to a plastic strain control mechanism. In more details, one can argue that applied stress may stimulate an increase in the ME- response in two ways: primarily by elastic stress – induced effects [18,19] and secondarily by flow stress- assisted and plastic strain – induced axial deformation texture [19,20]. Although the contribution in the second way is quite lower it should not be ignored. Thus, this contribution may be possible by complicated grain sliding and rotations each slip system in the individual grains of polycrystalline steel taking place during plastic flow. The superposition of these events, gives rise to the final orientation of grains resulting in an overall reduction of average disorientation. In this manner, any axial plastic deformation produces a more or less complete axial texture in which most of grains show a definite orientation along the axis of applied stress but occupy random

positions around this. With respect to this, in iron for example, the most probable texture is in the crystallographic direction $\langle 110 \rangle$ [22, 23]. It is noted that similar but a more complete and distinct tensile texture forms on heavy plastic deformations typical of a neck up to fracture [8, 22]. The essential result all of this is a local reorientation of magnetic easy axis which may reduce considerable the magnetoelastic or stray (demagnetization) fields interaction between magnetic domains. This is because two neighboring grains with interaction easy axis orthogonal to one another can reorient so that their directions may come closer each other or even become parallel. This reduce the closure domain flux and hence the formation of supplementary domains at grain boundaries thus allowing a much more easy passage of domains walls from grain to grain in creating a larger region of a correlated- cooperative domain activity [2,19]. This, in turn, leads to a net increase in the rate of local magnetic volume change and hence to an increase in the related ME- response. However, beyond the critical strain point, within the region II*, the magnetic response is controlled by plastic strain – induced volume damage. It is noted that the elastoplastic damage induced in this way is a complex entity involving not only the nucleation and growth of cavities and microcracks, but also their coupling with the strain – hardening effects or with strain localization due to large deformation [24]. Thus, at maximum response point the critical damage accumulation in form of new internal open surfaces may act as additional energy barriers by pinning at place many domain walls and reduce the ME-response. Furthermore, beyond this maximum point although the true tensile stresses continue to increase with higher rate their effects can no longer dominate over those of volume damage, admitting the later to take over in the competing process of magnetic response. This could further be explained by an additional contribution of (long –range) stress concentration gradient fields developed around preexisting inhomogenities such as grain boundaries and inclusions as well as

new created microcracks and nodal dislocation tangles of forming cell network. In this aspect, these fields tend to destabilize the local magnetization vector by impeding its redistribution towards axis closest oriented to macroscopic applied stress and magnetization direction. Regarding the above behavior in region II* we mention at this place that the above described plastic strain –affected micromagnetic structure simulates the behavior of magnetically hard materials which is controlled by the presence of microstructural inhomogenities or discontinuities in form of internal residue or active stresses, voids, cavities, microcracks, dislocation tangles, inclusions etc. [23]. As such, these inhomogenities are factors which govern the size, mobility and distribution of magnetic domains in hard magnetic materials [19,23,25]. Nevertheless, the correct interpretation of ME- response, especially of plastic strain – induced microstructural changes, is dependent on, as well as several aspects of the Barkhausen emission phenomenon concerning source mechanisms electromagnetic wave propagation and detection of induced elementary micromagnetic events as described in [26-27].

Thereafter, because beyond the above – discussed critical magnetic response strain point, e^*_c the influence of these factors seems to change significantly one can argue that this point could reflex a transition from a decreasing magnetic hardening (region I*) to an increasing magnetic hardening tendency (region II*) of material. However, the decreasing magnetic hardening is equivalent to an increase in the magnetic softening and in this sense one could argue that a possible high limiting value of $j^{(max)}$ at this point may simulate the existence of a stressed soft magnetic material of perm alloy-type, characterized by a high differential permeability. By following the principle of the earlier introduced mechanical response number, one may now adopt a reduced form of obtained data by which magnetic and mechanical response sensitivity number as given by the parameters: $\bar{n}^* =$

e^*_{co}/e^*_{ci} and $\bar{n} = \varepsilon_{co}/\varepsilon_{ci}$ respectively are expressed.

In these expression e^*_{co} and ε_{co} is the earlier introduced critical magnetic and mechanical response strain for the initial, $t_i = 0$, hydrogen-free state, whereas e^*_{ci} and ε_{ci} the respective critical response strain for the states of hydrogen accumulation for exposure time $t_i > 0$. Moreover, as earlier explained concerning the mechanical response number, the above form of reduced parameter may simulate a respective time scaling process in the sense that an increase (decrease) in these sensitivity parameters the critical damage accumulation can be “seen” or “detected” in an earlier (later) stage of progressive plastic deformation. In other words, these parameters could reflect a kind of a response sensitivity or ability in determining the degree of proneness or susceptibility to magnetic hardening (softening) of the material. From the series of figures (5a, b, c, d) one can observe the evident shift of magnetic and critical strain points e^*_c and e_u respectively to lower values with time of hydrogen accumulation. By measuring this shift, one can calculate the above introduced reduced response sensitivities humbers \bar{n}^* and \bar{n} . For better comparison the calculated response sensitivities numbers are plotted together in fig (6), where the slope of each curve reflects the rate of change of the related response. From this slope, the relative greater sensitivity of the magnetic response in early detecting hydrogen-assisted damaging processes especially for high accumulation, can be deduced. This is an interesting finding which indicates that the immobilization rate of domain walls due to hydrogen damage may become much higher than the rate of hydrogen damage-induced micromechanical degradation of material. Further details concerning the variation of these sensitivities can be obtained from figure (7) where evolution of the specific expression of these variables with time of hydrogen accumulation is shown.

These specific expressions are obtained by means of the reduce parameters as given by $\bar{S} = \frac{\bar{n}}{\bar{\sigma}^{max}}$ and $\bar{S}^* = \frac{\bar{n}^*}{j^{max}}$ where here

$$\bar{\sigma}_i^{max} = \frac{\sigma_i^{max}}{\sigma_o^{max}} \quad \text{and} \quad \bar{j}^{max} = \frac{j_i^{max}}{j_o^{max}}$$

Further, σ_o^{max} and σ_i^{max} is the maximum, ultimate tensile strength (stress), obtained by figure (2), for initial, hydrogen-free and for the following hydrogen-accumulation states for times $t_i=0$ and $t_i>0$ respectively; j_o^{max} and j_i^{max} is the maximum value of the absolute, stress-free, ME- response for initial (hydrogen-free) state and for hydrogen accumulation state for times $t_i=0$ and $t_i>0$ respectively. With respect to this, the specific sensitivities may provide a further valuable reference basis for comparison of hydrogen processes because in this way the evolution of initially given response state is analyzed on the basis of its current value of a maximum hydrogen influence where, as earlier explained, certain critical microstructural changes take place.

In this sense, from figure (7), the superior specific sensitivity of magnetic response over the mechanical one in early detecting hydrogen damage once again can be deduced. This superiority becomes more evident for high hydrogen accumulation times above about 800 hrs.

In the following, we will use the reduced maximum value for the ME-response to discuss some further interesting factors of hydrogen-assisted processes taking place in stressed steel.

Thus, we proceed as follows: the parameter

$$\bar{j}_{\sigma,\varepsilon,h,h^*}^{max} = \frac{j_{\sigma,\varepsilon,h,h^*}^{max}}{j_o}$$

expresses differential sensitivity in form of the reduced global-affected maximum ME-response as a function of all the influential factors denoted by subscripts of applied stress (σ), strain (ε), diffusional hydrogen accumulation (h) and dislocation-transported hydrogen (h^*). This reference parameter j_o reflects the initial absolute ME-response parameters of virgin, i.e. non-corroded and non-stressed material. In similar way of this reduction procedure one can introduce some variants of reduced ME-response as follows: $\bar{j}_h = \frac{j_{(t \geq 0)}}{j_o}$ expressing the reduced ME-response of the influence of diffusional hydrogen accumulation. As such, the reduction of the global ME-response to the \bar{j}_h gives,

$\bar{j}_{\sigma,\varepsilon,h,h^*}^{max} / \bar{j}_h = \bar{j}_{\sigma,\varepsilon,h^*}^{max}$ where the influence of diffusional hydrogen accumulation (h), expressed by j'_h , was “discriminated”. By the following reduction one may further obtain $\bar{j}_{\varepsilon,h,h^*}^{max} = \frac{j_{\varepsilon,h,h^*}^{max}}{j_{\sigma}^{max}}$ where the influence of ultimate stress was “discriminated”. This is possible because as seen in Figure (2) this stress changes very little with corrosion (hydrogen accumulation) time and as such is assumed to have the same value for all corrosion times.

Afterwards one can formally further obtain $\bar{j}_{\varepsilon,h^*}^{max} = \frac{j_{\varepsilon,h,h^*}^{max}}{\bar{j}_h}$, where the influence of the diffusional hydrogen, \bar{j}_h , was “discriminated”.

Thereafter, in figure (8), the differential complete or opposing influence of the above-mentioned factors is presented.

Thus, the observed initial and following overall shift of the global ME-response curve, $\bar{j}_{\sigma,\varepsilon,h,h^*}^{max}$, upwards from \bar{j}_h -ME-response curve is an interesting indicator of the strong dominance of applied stress over the combined effect of all the other three influential factors of plastic strain (ε), diffusional (h) and dislocation-transported cumulative hydrogen (h^*). This is because, as earlier explained, the factors of plastic strain (ε) and hydrogen accumulation (h,h^*) are opposed to the applied stress effects in reducing the ME-response strength and the increasing the magnetic hardening tendency of material. In other words, the above findings could reflect a state of an applied tensile stress-triggered magnetic hardening delay of material. Furthermore, by comparing the curves $\bar{j}_{\sigma,\varepsilon,h^*}^{max}$ and $\bar{j}_{\varepsilon,h,h^*}$ an overall shift of both curves, of almost same extent, upwards and downwards respectively from maximum global-ME-response curve, $\bar{j}_{\sigma,\varepsilon,h,h^*}^{max}$ can be observed. This behavior reflects, the essential confirmation that the applied tensile stress and diffusional cumulative hydrogen are opposite processes in affecting the ME-response. Nevertheless, this finding can further be examined by means of curve $\bar{j}_{\varepsilon,h^*}^{max}$ by which the combined effect of applied stress (σ) and diffusional

cumulative hydrogen (h) was “discriminated”, through the earlier mentioned reduction procedure. Since, as it was confirmed above, applied stress and diffusional hydrogen are opposing effects, the observed shift of the maximum global-ME-response curve, $\bar{j}_{\sigma,\varepsilon,h,h^*}^{max}$, although slightly, upwards from curve $\bar{j}_{\varepsilon,h^*}^{max}$ may be clear evidence of the dominance of the tensile stress (σ) factor over the diffusional (h) and plastic strain factor (ε) resulting in an increase in the specific ME-response.

Moreover, one can go a step further by examining the influence of the residual compressive stress factor, on ME-response. This is done by investigating the ME-response behavior of specimens after unloading at ultimate stress short before the necking formation. This is expressed by the curve of parameter $\bar{j}_{\sigma^-, \varepsilon, h, h^*}$, where subscript σ^- denotes influence of compressive negative, stresses.

Thus, critical damage accumulation prior unloading can be seen to be equivalent to damage “remaining” after ultimate unloading. This implies that any changes of related ME-response before and after ultimate unloading should be a function solely of variables of tensile stress (σ) and compressive stress (σ^-) influential factors. Therefore, it is interesting to observe, in figure (8), the overall shift of ME-response curve of ultimate unloaded specimens, $\bar{j}_{\sigma^-, \varepsilon, h, h^*}$ downwards, to lower values of ME-response curve \bar{j}_h . At the same time by observing the overall shift of the global -ME-response curve $\bar{j}_{\sigma^-, \varepsilon, h, h^*}^{max}$ upwards from curve \bar{j}_h , one can deduce the opposite effect of compressive stresses compared with tensile stresses in suppressing the ME-response, fact equivalent to a stimulation of a magnetic hardening tendency of material. This can be explained by the characteristics fact that after ultimate unloading, permanent (residual) internal compressive stresses, mainly within the surface and subsurface layers of specimen, are created [15 – 17, 25, 26]. In our case this could be explained as follows:

With increasing time of hydrogen accumulation the following opposing processes may occur. Stress-relief effects increase their contribution by reducing the

on-load tensile stress concentration gradient fields resulting in an associated reduction in residual compressive stress gradients created subsequently after ultimate unloading at prior tensile stress gradients sites. Furthermore, due to the increase in hydrogen-assisted damage, an increase in the portion of new (open) internal surfaces arises. Now, the compressive stress fields developed after ultimate unloading exhibit a closure effect on these surfaces which tend to become partially or totally closed. However, due to the stress relief-weakened compressive stresses a net increase of the portion of semi open surfaces results. This in turn would lead to an increase in magnetic stray field density which acting as additional pinning sites for domain walls may result in a net decrease of the measured ME-responses. However, at the same time, the increased stress-relief effect tend to reduce the magnetoelastic -magnetostreictive interaction of magnetic domains with pinning sites, fact which would increase the related ME-response with time of hydrogen accumulation. Thus, the net result of the dominating volume damage effects lead to a reduction in the ME-response. Finally, in Fig (9) the evolution of the $\bar{j}_{\sigma^-, \varepsilon, h, h^*}$ parameter with corrosion time is presented. This was evaluated after fracture of specimen by measurements taken within the ultimate necking region. One can clearly observe the overall shift of this parameter to lower level of micromagnetic activity compared with all curves of Fig 8. In a first instance this is indicative of the stronger dominance of the above-explained volume damage effects within ultimate necking region. Furthermore, as earlier explained, necking as a plastic instability phenomenon, is characterized, among others, by production of extended volume damage in form large dimples, cavities, voids and crack-like defects. [8, 22]. Consequently, after fracture unloading the total net surface of open and/or partially open volume damage is considerably increased fact which would lead to strong barriers for moving domain walls. At this microstructural state level the hydrogen accumulation-induced closure compression stress relief favourises a

quasiequilibrated behavior of micromagnetic activity expressed, as seen in Fig 9, by the related almost constant parameter.

IV CONCLUSION

From the present investigation the following essential conclusions can be extracted. By means of a combined approach for the cumulative hydrogen influence on the mutual tensile mechanical and micro magnetic emission response, it was possible to obtain several valuable information about hydrogen-assisted pervasive damaging processes in a loaded steel. This task can optimally be performed by introducing certain relevant parameters related to inherent mechanical and ferromagnetic microstructural changes. The first of these is the reduced \bar{j} - parameter by which the changes of the ME-response with hydrogen accumulation is expressed by this parameter, in turn, other relevant ones are introduced, such as the mechanical and magnetic emission response sensitivity by which the onset and strength of critical plastic damage and of micromagnetic activity respectively are determined. At the same time the specific magnetic emission response sensitivity reflecting maximum rate of change of micromagnetic activity and hence of displacement strength of domain walls were introduced. In this way one can in a first instance show that cumulative hydrogen may assist in occurrence of mechanical embrittlement process by means of lattice diffusion-aided as well as moving dislocation – aided hydrogen transport to the affected sites, at which, afterwards, highly localized opposing mechanisms of void growth and stress-relief are activated. In principle one can show that by applying a tensile stress certain valuable effects of mutual micro

magnetic emission and plastic strain-induced microstructural response on cumulative hydrogen influence may be obtained. These effects can be evaluated by an adequate procedure consisting in a series of “consecutive discrimination steps” of the related affecting factors by which the selective-differential influence of hydrogen accumulation can better be revealed and analyzed. In this aspect the opposite effect of tensile stress and residual compressive stresses in affecting the ME-response on hydrogen accumulation was reasonably demonstrated. As such, under hydrogen influence tensile stress seems to stimulate a magnetic hardening depression whereas residual compressive stresses a magnetic hardening tendency. In the frame of the above findings the greater sensitivity of ME-response, compared with mechanical one, can be estimated making the first a superior non-destructive testing technique for early detecting hydrogen-assisted damaging processes taking place in steel components under stress. In general, it seems that the presented combined approach may provide an investigation tool by means of a mutual applied mechanical and micro magnetic emission response.

REFERENCE

- [1]. “Physical Methods for Materials Characterization”, Institute of Physics Publishing Bristol and Philadelphia, 1994.
- [2]. Martha Pardari -Horvath, “Magnetic Noise, Barkhausen Effect”, in Wily Encyclopedia of Electrical and Engineering, Vol. 12, pp.52-64, J. G Webster, Ed.
- [3]. Noyan, I. C, Cohen J.B. Residual stress, measurement

- by diffraction and interpretation. New York: Springer, 1987, p276.
- [4]. H. Moller, E.T. Boshoff, and H. Foreman, "The corrosion Behavior of a low- carbon steel in natural and synthetic seawaters "The journal of South African Institute of Mining and Metallurgy, Vol. 106, pp.585-592, 2005.
- [5]. Hydrogen Embrittlement of low Carbon HSLA Steel during slow Strain Rate Test, Yingwei Zhao, Young SOO Chun and Chong SOO Lee , Advanced Materials Research, Val's 197-198, (2011) pp. 642-645.
- [6]. E.K.Ioakeimeidis , V.N.Kytopoulos, E. Hristoforou " Investigation of magnetic, mechanical and micro failure Barkhausen of ARMCO – type LOW-Carbon steel corroded in 3,5% NaCl –aqueous solution " Mat. Sci. Eng: A, Vol.583, 2013, pp.254-260.
- [7]. E.k. Ioakeimidis "Correlation of microstructure, mechanical and magnetical properties of low carbon steel. Study of the influence of the electrochemical and chemical corrosion on the mechanical and magnetical behavior of ARMCO- type steel, Ph.D. Thesis, NTUA Greece, 2013." , 3d Ed. Willeg, 1989.
- [8]. R. W .Herzberg, "Deformation and Fracture Mechanisms of Engineering Materials", 3d Ed. Willeg 1989.
- [9]. T. Alan Place , T. Srinivas Subur Cindy Waters and M.R. Louthan , " Fractographic Studies of ductile – to – Brittle Transition in AUSTENITIC Stainless Steels in Fractography of Modern Engineering Materials: Composites and Metals, Eds. Master, J. and Au, J., ASTM-STP 948, pp.350-365.
- [10]. Yoneo Riruta, Takqo Araki, and Toshio Kuroda , " Analysis of Fracture Morphology of Hydrogen – Assisted Cracking in Steel and Welds ", in Fractography in failure analysis , ASTM – STP 645, 1978, pp.107-127.
- [11]. Daas, A.K. "Metallurgy of Failure Analysis, "Mc Graw-Hill, 1996, 18-A. Hubert and R. Schafer, "Magnetic Domains. The Analysis of Magnetic structure. "Corrected Printing 2000, Springer.
- [12]. C.L. Briant, "Metallurgical Aspects of Environmental Failures ", Materials Science Monographs, Vol. 12, Elsevier, 1985.
- [13]. Doling, N.E., Mechanical Behavior of Materials, Engineering Methods for Deformation, Fracture and Fatigue. Prentic- Hall International Editions, 1993.
- [14]. Joshi , A., " Role of Interface chemistry in Failure of Materials " , in Fractography in Failure Analysis , ASTM-STP 645, 1945, Eds Strains / Cullen.
- [15]. Sullivan D. Cotterel M.Tanner Meszaros I. " Characterization of ferritic stainless steel by Barkhausen techniques NDT& E. International, Vol.37, Issue 6, September 2004, Pages 489-496.
- [16]. A. Dhar, I. Clapham, D.L.Atherton, "The influence

- of pearlite on magnetic emission in plain carbon steels, NDT and E. International 5 (29), 338.
- [17]. Lindgren M. Lepisto T. Effect of prestrain on Barkhausen Noise vs stress relation NDT & E. International, Vol. 34, Issue 5, July 2001, pp 337-344.
- [18]. C. E. Stefanita, L. Clapham, and D.L. Atherton, "Subtle changes in magnetic Barkhausen noise before the macroscopic elastic Limit ", J.Mat. Sci, 35, pp.2675-2681, (2000).
- [19]. T.W. Krause, L. Clapham, Apattantyns, and D.L.Atherton, Investigation of the stress- dependent magnetic easy axis in steel using magnetic Barkhausen noise", J.Appl. Phys., 79,(8), 4242-4252,(1996).
- [20]. D. G.Hwang and H.C.Kim, "The influence of plastic deformation on Barkhausen effect and magnetic properties in mild Steel, J. Phys. D: Appl. Phys. (1988), pp.1807—1813.
- [21]. Stefanita C.G., Atherton D.L., Clapham L., Acta Mater 2000, Vol.48 (13), pp.3545-3551.
- [22]. P. Polukhin, S. Gorelik and V.Vorontsov "Physical Principles of Plastic Deformation, Mir Publishers, Moscow, 1983.
- [23]. S. Chikazsmi, "Physics of Ferromagnetism, "Second Edition, Oxford Science Publishers, 1997.
- [24]. Murakami Sumio, " Anisotropic Aspects of Material Damage and Application of Continuum Damage Mechanic ", in Continuum Damage Mechanics, Theory and Application , Eds D. Krejcinovic and J. Lemaitre , Springe Verlag Wien – New York, 1987.
- [25]. Humbert A. and Schafer R. Magnetic Domain, "The analysis of magnetic structure». Corrected Printing 2000 Springer.
- [26]. Mohamed Blaow, John. T. Evans and B.A. Shaw," The effect of microstructure and applied stress on magnetic Barkhausen emission in induction hardened Steel ", J. Mat. Sci. (2007) 42, pp. 4364-4371.
- [27]. O. Saquet, J.Chicois, A. Vincent, "Barkhausen noise from plain carbon steels: analysis of the influence of microstructure, "Mat. Sci. and Engineering, A269 (1999), pp. 73-83.

FIGURE CAPTIONS

Figure 1. Schematic of Block diagram of used magnetic Barkhausen set up.

Figure 2. Engineering stress-strain curves, obtained for several given times of corrosion or hydrogen accumulation.

Figure 3. Measured magnetic Barkhausen counts and rms- voltage signal in function of operative-applied tensile strain.

Fig 4. Absolute magnetic Barkhausen response parameter plotted against time of hydrogen accumulation (corrosion).

Figure 5(a).Applied tensile stress and absolute ME-response parameter plotted against operative strain for initial, corrosion (hydrogen –free) condition.

Figure 5(b). Applied tensile stress and absolute ME-response parameter plotted against strain for 200 hours of the hydrogen accumulation (corrosion).

Figure 5(c). Applied tensile stress and absolute ME-response parameter plotted against strain for 600

hours of the hydrogen accumulation (corrosion).

Figure 5(d). Applied tensile stress and absolute ME-response parameter plotted against strain for 1000 hours of the hydrogen accumulation (corrosion).

Figure 6. ME-response sensitivity numbers plotted against time of hydrogen accumulation (corrosion).

Figure 7. Specific ME-response sensitivity plotted against time of hydrogen accumulation (corrosion).

Figure 8. Differential influence on the ME-response plotted against time of hydrogen accumulation

(corrosion).

Figure 9. Evolution of Compression stress-affected specific sensitivity with time of corrosion (hydrogen accumulation) after fracture unloading.

Table1. The chemical composition of used low-carbon steel (%)

Creative Commons Attribution License 4.0 (Attribution 4.0 International, CC BY 4.0)

This article is published under the terms of the Creative Commons Attribution License 4.0

https://creativecommons.org/licenses/by/4.0/deed.en_US

Figure 1:

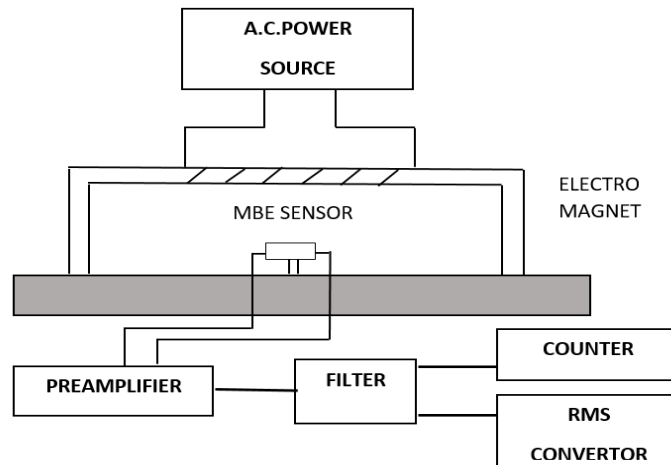


Figure 2:

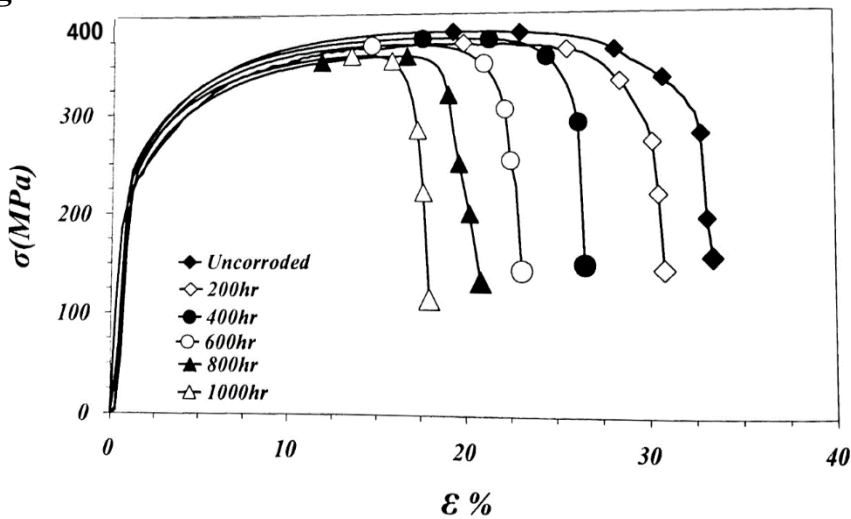


Figure 3:

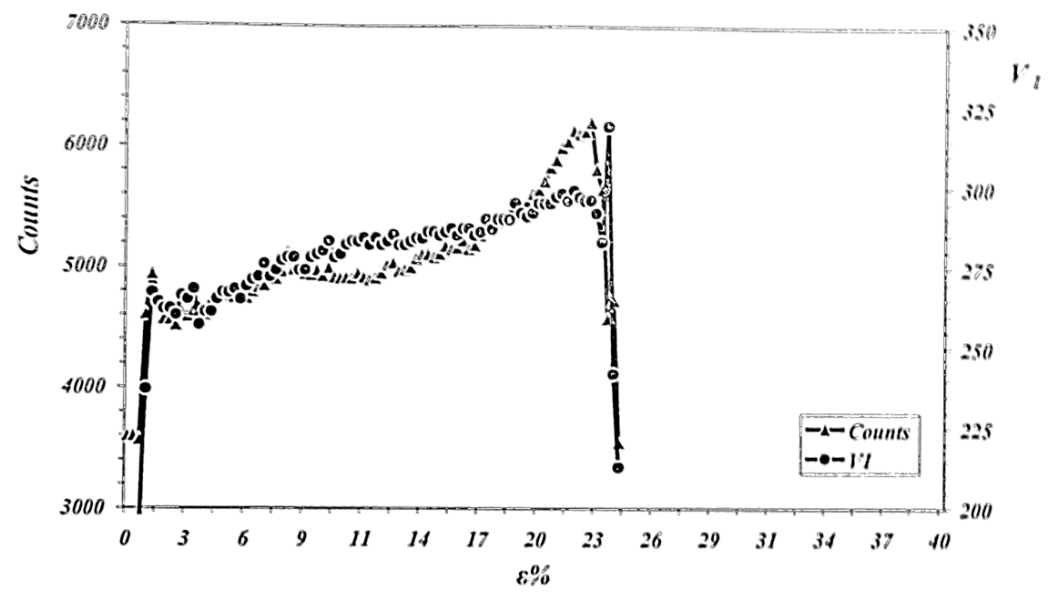


Figure 4:

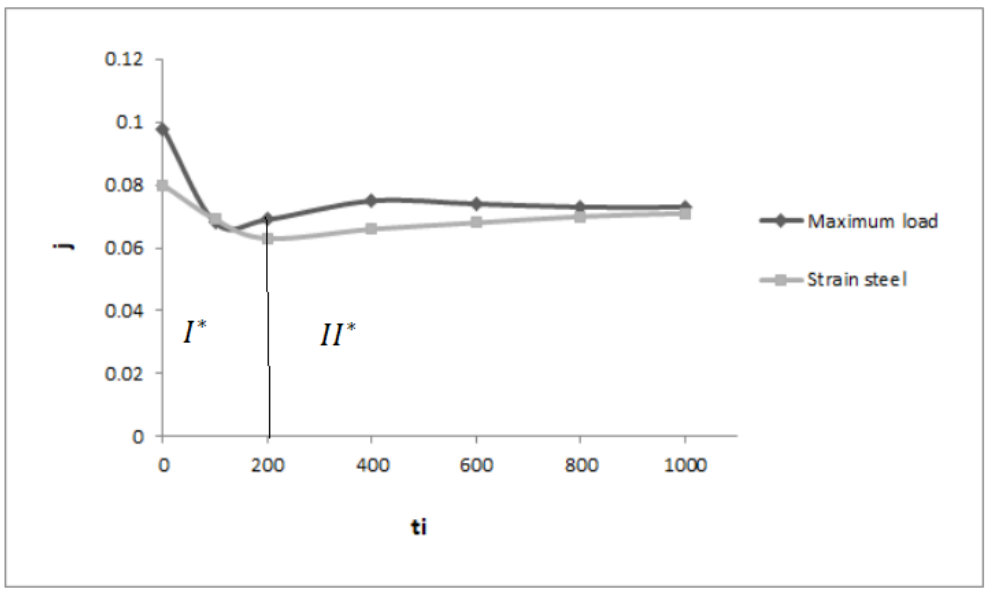


Figure 5(a):

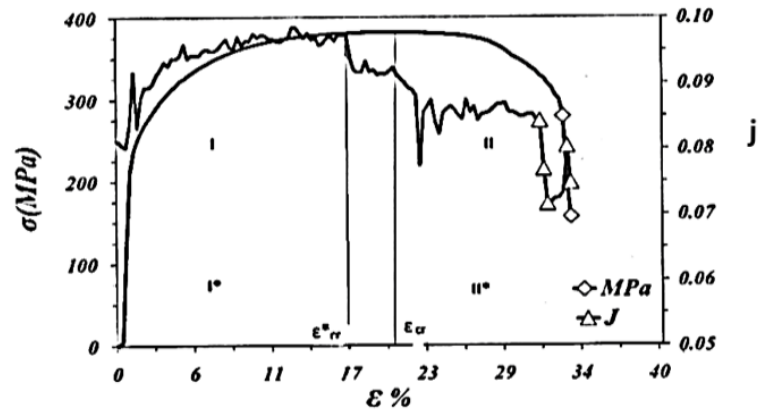


Figure 5(b):

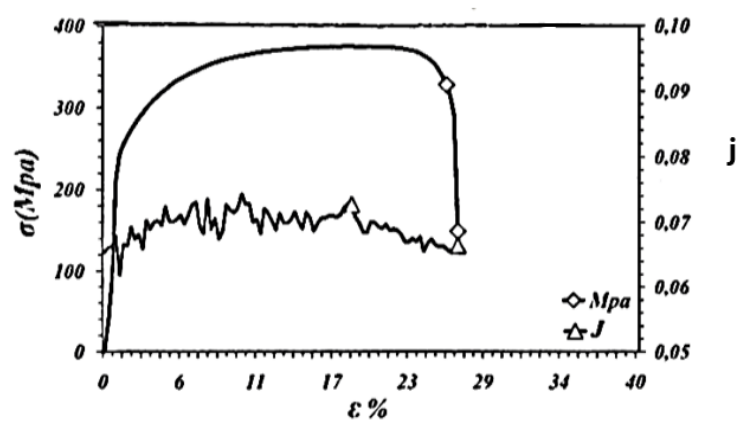


Figure 5c:

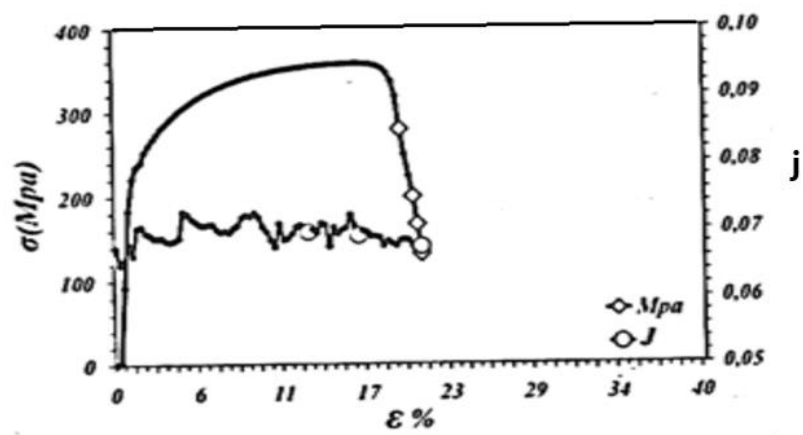


Figure 5(d):

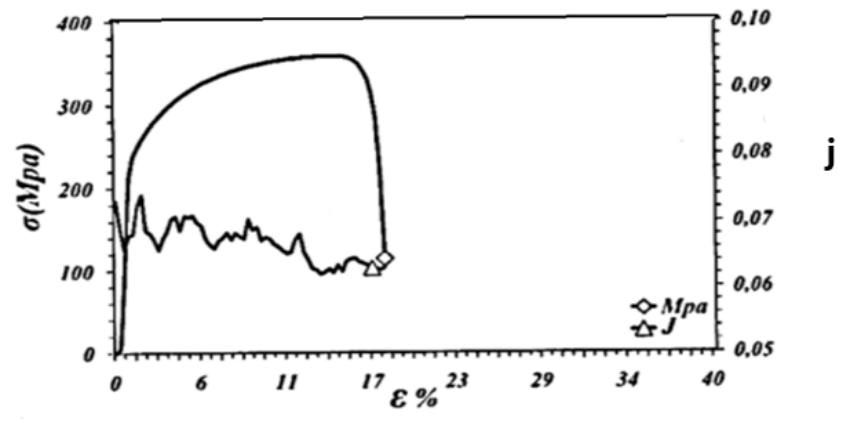


Figure 6:

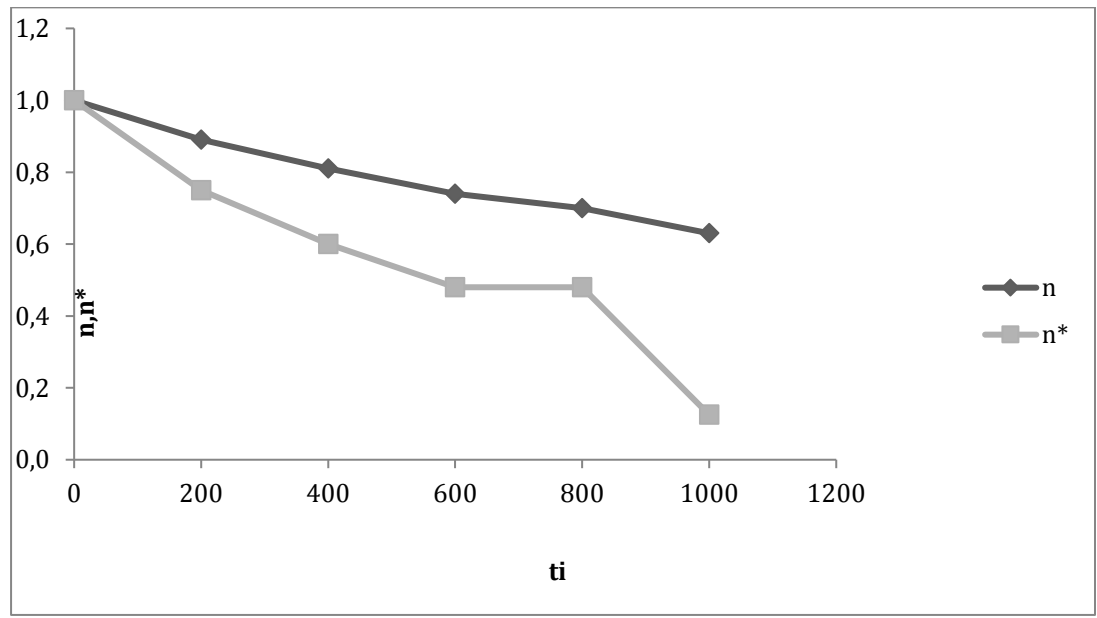


Figure 7:

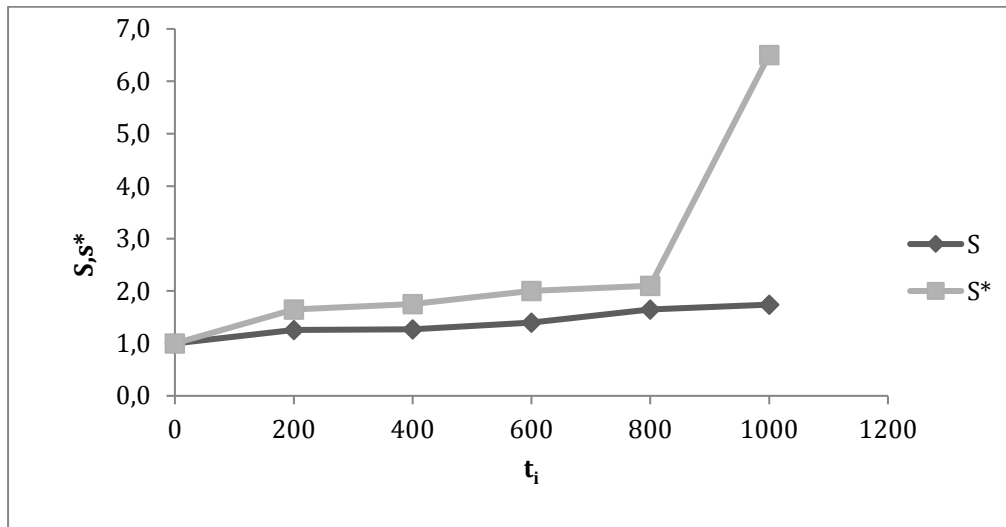


Figure 8:

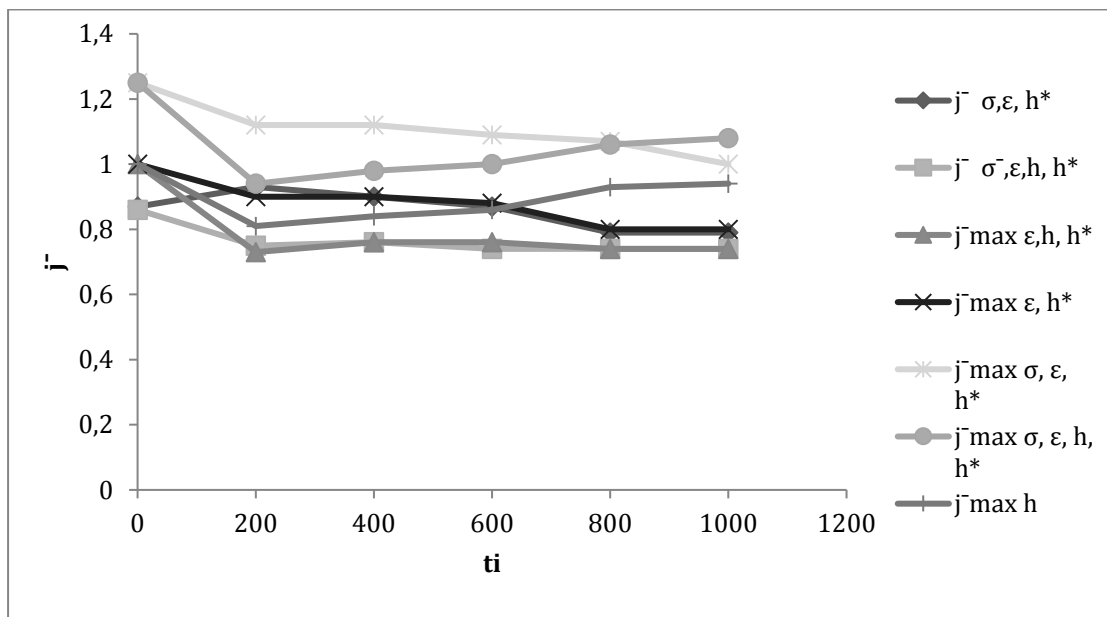


Figure 9:

